Available online at www.sciencedirect.com
SCIENCE DIRECT®
Journal of Solid State Chemistry 175 (2003) 264–271
JOURNAL OF SOLID STATE CHEMISTRY
http://elsevier.com/locate/jssc

Synthesis, characterization and dielectric properties of new unidimensional quaternary tellurites: $LaTeNbO_6$, $La_4Te_6Nb_2O_{23}$, and $La_4Te_6Ta_2O_{23}$

Kang Min Ok, Lei Zhang, and P. Shiv Halasyamani*

Department of Chemistry and Center for Materials Chemistry, University of Houston, 136 Fleming Building, 4800 Calhoun Blvd., Houston, TX 77204-5003, USA

Received 4 March 2003; received in revised form 29 April 2003; accepted 7 May 2003

Abstract

Three new tellurites, $LaTeNbO_6$ and $La_4Te_6M_2O_{23}$ (M = Nb or Ta) have been synthesized, as bulk phase powders and crystals, by using La_2O_3, Nb_2O_5 (or Ta_2O_5), and TeO_2 as reagents. The structures of $LaTeNbO_6$ and $La_4Te_6Ta_2O_{23}$ were determined by single crystal X-ray diffraction. $LaTeNbO_6$ consists of one-dimensional corner-linked chains of NbO_6 octahedra that are connected by TeO_3 polyhedra. $La_4Te_6M_2O_{23}$ (M = Nb or Ta) is composed of corner-linked chains of MO_6 octahedra that are also connected by TeO_4 and two TeO_3 polyhedra. In all of the reported materials, Te^{4+} is in an asymmetric coordination environment attributable to its stereo-active lone-pair. Infrared, thermogravimetric, and dielectric analyses are also presented. Crystallographic information: $LaTeNbO_6$, triclinic, space group $P-1$, $a = 6.7842(6)$ Å, $b = 7.4473(6)$ Å, $c = 10.7519(9)$ Å, $\alpha = 79.6490(10)°$, $\beta = 76.920(2)°$, $\gamma = 89.923(2)°$, $Z = 4$; $La_4Te_6Ta_2O_{23}$, monoclinic, space group $C2/c$, $a = 23.4676(17)$ Å, $b = 12.1291(9)$ Å, $c = 7.6416(6)$ Å, $\beta = 101.2580(10)°$, $Z = 4$.

Keywords: Oxides; Tellurites; One-dimensional; Dielectric properties; X-ray diffraction

1. Introduction

Mixed-metal tellurites (Te^{4+}) have a rich structural chemistry attributable to their stereo-active lone-pair as well as their variable coordination environments. The stereo-active lone-pair is thought to be the result of a second-order Jahn–Teller (SOJT) distortion [1–5]. The SOJT distortion reduces the energy of the highest occupied (HOMO) s-orbital by mixing with the lowest unoccupied (LUMO) p-orbital, i.e. $s-p$ mixing, resulting in the stereo-active lone-pair. Structurally, the lone-pair creates an asymmetric coordination environment for Te^{4+}. With respect to oxide bonding, Te^{4+} may be three-, four-, or five-coordinate. In connectivity terms, the coordination can range from fully bonding, e.g. $[TeO_{4/2}]^0$ and $[TeO_{3/2}]^+$, to completely terminal, e.g. $[TeO_{3/1}]^{2-}$ [6,7]. We have been interested in combining the asymmetric environment and variable coordination of Te^{4+} with other SOJT distorted cations, e.g. d^0 transition metals (Ti^{4+}, Nb^{5+}, or W^{6+}). In doing so, our aim is to not only create new materials, but also to synthesize non-centrosymmetric materials in order to investigate their non-linear optical properties [8]. In this paper, we report the syntheses, structures and dielectric behavior of three new mixed-metal tellurites, $LaTeNbO_6$ and $La_4Te_6M_2O_{23}$ (M = Nb or Ta).

2. Experimental

2.1. Reagents

TeO_2 (Aldrich, 99%), Nb_2O_5 (Aldrich, 99.99%), and Ta_2O_5 (Alfa Aesar, 99%) were used as received. La_2O_3 (Aldrich, 99.9%) was dried overnight at 1000°C before being used.

2.2. Syntheses

2.2.1. Bulk phase powder

For $LaTeNbO_6$, 0.724 g (2.22×10^{-3} mol) of La_2O_3, 0.591 g (2.22×10^{-3} mol) of Nb_2O_5, and 0.709 g

*Corresponding author. Fax: +713-743-2787.
E-mail address: psh@uh.edu (P.S. Halasyamani).

0022-4596/03/$ - see front matter © 2003 Elsevier Inc. All rights reserved.
doi:10.1016/S0022-4596(03)00260-3

(4.44×10^{-3} mol) of TeO_2 were combined. For $La_4Te_6Nb_2O_{23}$, 1.417 g (4.35×10^{-3} mol) of La_2O_3, 0.578 g (2.17×10^{-3} mol) of Nb_2O_5, and 2.082 g (13.05×10^{-3} mol) of TeO_2 were combined. For $La_4Te_6Ta_2O_{23}$, 1.303 g (4.00×10^{-3} mol) of La_2O_3, 0.884 g (2.00×10^{-3} mol) of Ta_2O_5, and 1.915 g (12.00×10^{-3} mol) of TeO_2 were combined. The respective mixtures were thoroughly ground with an agate mortar and pestle and pressed into pellets. The pellets were introduced into quartz tubes that were subsequently evacuated and sealed. For $LaTeNbO_6$, the tube was heated to 850°C for 60 h and cooled to room temperature with two intermittent re-grindings. $La_4Te_6M_2O_{23}$ (M = Nb or Ta) was heated to 800°C for 48 h and cooled to room temperature with one intermediate re-grinding. Powder X-ray diffraction patterns on the resultant white powders indicated each material was single phase.

2.2.2. Single crystals

For $LaTeNbO_6$, 0.421 g (1.29×10^{-3} mol) of La_2O_3, 0.343 g (1.29×10^{-3} mol) of Nb_2O_5, and 1.236 g (7.74×10^{-3} mol) of TeO_2 were combined. For $La_4Te_6Nb_2O_{23}$, 0.326 g (1.00×10^{-3} mol) of La_2O_3, 0.133 g (0.50×10^{-3} mol) of Nb_2O_5, and 0.958 g (6.00×10^{-3} mol) of TeO_2 were combined. For $La_4Te_6Ta_2O_{23}$, 0.192 g (0.59×10^{-3} mol) of La_2O_3, 0.130 g (0.29×10^{-3} mol) of Ta_2O_5, and 0.563 g (3.53×10^{-3} mol) of TeO_2 were combined. Excess TeO_2 was added in order to promote crystal growth. The respective mixtures were thoroughly ground with an agate mortar and pestle and introduced into separate gold tubes that were subsequently sealed. The gold tubes were heated to 900°C for 24 h and then cooled to 500°C at 6°C h^{-1} before being quenched to room temperature. Crystals of $LaTeNbO_6$ (colorless rods) and $La_4Te_6M_2O_{23}$ (M = Nb or Ta; colorless blocks) were recovered from each gold tube. Crystals of $La_4Te_6Ta_2O_{23}$ were of much better quality than $La_4Te_6Nb_2O_{23}$; thus the former were used for single crystal analysis. Powder X-ray diffraction was used to show $La_4Te_6Nb_2O_{23}$ is iso-structural to $La_4Te_6Ta_2O_{23}$. Powder X-ray diffraction patterns for each material is in agreement with the generated patterns from the single crystal data (see Supporting Information).

2.3. Crystallographic determination

A colorless rod (approximate size: $0.02 \times 0.02 \times 0.30$ mm) for $LaTeNbO_6$ and a colorless block (approximate size: $0.10 \times 0.10 \times 0.15$ mm) for $La_4Te_6Ta_2O_{23}$ were used for single crystal data analyses. Room temperature intensity data were collected on a Siemens SMART diffractometer equipped with a 1 K CCD area detector using graphite monochromated Mo$K\alpha$ radiation. A hemisphere of data was collected using a narrow-frame method with scan widths of 0.30° in omega, and an exposure time of 25 s/frame. The first 50 frames were re-measured at the end of the data collection to monitor instrument and crystal stability. The maximum correction applied to the intensities was <1%. The data were integrated using the Siemens SAINT program [9], with the intensities corrected for Lorentz, polarization, air absorption, and absorption attributable to the variation in the path length through the detector faceplate. Psi-scans were used for the absorption correction on the hemisphere of data. The data were solved and refined using SHELXS-97 and SHELXL-97, respectively [10,11]. All of the atoms were refined with anisotropic thermal parameters and converged for $I > 2\sigma(I)$. All calculations were performed using the WinGX-98 crystallographic software package [12]. Crystallographic data, atomic coordinates and thermal parameters, and selected bond distances for $LaTeNbO_6$ and $La_4Te_6Ta_2O_{23}$ are given in Tables 1–4.

Table 1
Crystallographic data for $LaTeNbO_6$ and $La_4Te_6Ta_2O_{23}$

	$LaTeNbO_6$	$La_4Te_6Ta_2O_{23}$
Formula weight	455.42	2051.14
Temperature (K)	293.0(2)	293.0(2)
Wavelength (Å)	0.71073	0.71073
Crystal system, space group	Triclinic, $P-1$ (No. 2)	Monoclinic, $C2/c$ (No. 15)
Unit cell dimensions	$a = 6.7842(6)$ Å	
$a = 23.4676(17)$ Å		
	$b = 7.4473(6)$ Å	
$b = 12.1291(9)$ Å		
$c = 10.7519(9)$ Å	$c = 7.6416(6)$ Å	
$\alpha = 79.6490(10)°$	$\alpha = 90°$	
	$\beta = 76.920(2)°$	
$\beta = 101.2580(10)°$		
	$\gamma = 89.923(2)°$	$\gamma = 90°$
Volume (Å^3), Z	520.08(8), 4	2133.3(3), 4
ρ_{calc}(g/cm^3)	5.82	6.39
θ Range (deg)	2.78–27.98	1.77–28.03
Absorption coeff. (mm^{-1})	15.76	26.196
Crystal size (mm)		
$0.02 \times 0.02 \times 0.30$		
$0.10 \times 0.10 \times 0.15$		
Refl. collected/unique	3206/2230 [R(int) = 0.0682]	6424/2424 [R(nit) = 0.0690]
Absorption correction	ψ-scan	ψ-scan
Refinement method	Full-matrix least-squares on F^2	Full-matrix least-squares on F^2
Goodness-of-fit on F^2	1.073	1.036
Final $R^{a,b}$ indices [$I > 2\sigma(I)$]	$R = 0.0432$, $R_w = 0.1168$	$R = 0.0353$, $R_w = 0.0951$
R indices (all data)	$R = 0.0487$, $R_w = 0.1205$	$R = 0.0427$, $R_w = 0.0984$
Extinction coefficient	0.0080(6)	0.00024(2)

[a] $R = \sum||F_o|-|F_c||/\sum|F_o|$.
[b] $R_w = [\sum w(F_o^2-F_c^2)^2/\sum w(F_o^2)^2]^{1/2}$.

In examining the thermal ellipsoid for Te(1) in $La_4Te_6Ta_2O_{23}$, we determined that this atom could be split over two sites, Te(1*a*) and Te(1*b*). In doing so, fractional occupancies of 0.52(4) and 0.48(4) were refined, respectively. During the course of the refinement for $La_4Te_6Ta_2O_{23}$, we also determined that fractional occupancy must occur in some of the oxygen atoms in order to retain charge balance. The possibility of Te^{6+} was considered, but quickly discarded owing to the asymmetric coordination environment of the tellurium cations, as well as the bond valence results (see Results and Discussion). Although a host of partial occupancy models are possible, only one makes structural sense. It seemed very unlikely that Ta^{5+} would at any time be five-coordinate; thus all of the oxygen atoms bonded to

Table 2
Atomic coordinates for $LaTeNbO_6$

Atom	*x*	*y*	*z*	U_{eq} (Å^2)
La(1)	0.3313(1)	0.2845(1)	0.8435(1)	0.009(1)
La(2)	0.7598(1)	0.8620(1)	0.4961(1)	0.011(1)
Te(1)	0.3299(1)	0.7982(1)	0.8008(1)	0.009(1)
Te(2)	0.7380(1)	0.3717(1)	0.4975(1)	0.010(1)
Nb(1)	0.8272(1)	0.0417(1)	0.8002(1)	0.008(1)
Nb(2)	0.8176(1)	0.5464(1)	0.8021(1)	0.009(1)
O(1)	0.5075(9)	0.9809(8)	0.8186(7)	0.016(1)
O(2)	0.1823(10)	0.0541(8)	0.0352(7)	0.016(1)
O(3)	0.8601(9)	0.8163(8)	0.7184(6)	0.014(1)
O(4)	0.8928(9)	0.8881(8)	0.2574(6)	0.011(1)
O(5)	0.8481(9)	0.1522(8)	0.5744(6)	0.013(1)
O(6)	0.7123(9)	0.2870(7)	0.8210(6)	0.013(1)
O(7)	0.1797(9)	0.4570(8)	0.4105(6)	0.014(1)
O(8)	0.5016(9)	0.6009(8)	0.7882(7)	0.016(1)
O(9)	0.0861(10)	0.5010(9)	0.7787(7)	0.020(2)
O(10)	0.2444(11)	0.4336(9)	0.0306(7)	0.022(2)
O(11)	0.3906(10)	0.8685(8)	0.6179(6)	0.015(1)
O(12)	0.5330(9)	0.6758(8)	0.4052(6)	0.011(1)

U_{eq} is defined as one-third of the trace of the orthogonalized U_{ij} tensor.

Table 4
Selected bond distances (Å) for $LaTeNbO_6$ and $La_4Te_6Ta_2O_{23}$

$LaTeNbO_6$		$La_4Te_6Ta_2O_{23}$	
Nb(1)–O(1)	2.173(6)	Ta(1)–O(1)	1.890(6)
Nb(1)–O(2)	1.772(7)	Ta(1)–O(2)	1.886(6)
Nb(1)–O(3)	2.019(6)	Ta(1)–O(3)	2.195(8)
Nb(1)–O(4)	1.903(6)	Ta(1)–O(4)	1.899(8)
Nb(1)–O(5)	2.391(7)	Ta(1)–O(4)	1.966(8)
Nb(1)–O(6)	2.015(5)	Ta(1)–O(5)	2.150(7)
Nb(2)–O(3)	2.042(6)	Te(1a)–O(3)	1.901(9)
Nb(2)–O(6)	2.020(6)	Te(1a)–O(6)	1.792(8)
Nb(2)–O(7)	2.287(7)	Te(1a)–O(7)	1.97(2)
Nb(2)–O(8)	2.215(6)	Te(1a)–O(7)′	2.44(2)
Nb(2)–O(9)	1.821(6)		
Nb(2)–O(10)	1.785(7)	Te(1b)–O(3)	1.839(8)
		Te(1b)–O(6)	1.904(10)
Te(1)–O(1)	1.882(6)	Te(1b)–O(7)′	1.91(2)
Te(1)–O(8)	1.879(6)	Te(1b)–O(7)	2.51(3)
Te(1)–O(11)	1.891(7)		
		Te(2)–O(8)	1.869(9)
Te(2)–O(5)	1.924(6)	Te(2)–O(9)	1.847(9)
Te(2)–O(7)	1.904(6)	Te(2)–O(10)	2.085(5)
Te(2)–O(12)	1.897(6)	Te(2)–O(11)	2.118(8)
		Te(3)–O(5)	1.906(8)
		Te(3)–O(12)	1.885(8)
		Te(3)–O(13)	1.885(8)

Table 3
Atomic coordinates for $La_4Te_6Ta_2O_{23}$

Atom	*x*	*y*	*z*	U_{eq}(Å^2)[a]	Occupancy
La(1)	0.17003(2)	0.24541(4)	0.08777(7)	0.00999(16)	1.0
La(2)	0.10110(3)	0.49929(4)	−0.21403(8)	0.01268(17)	1.0
Te(1a)	0.41733(12)	0.5116(5)	0.170(2)	0.0156(15)	0.52(4)
Te(1b)	0.41589(13)	0.4963(7)	0.235(2)	0.0165(16)	0.48(4)
Te(2)	−0.00094(3)	0.29317(6)	−0.00807(9)	0.01681(19)	1.0
Te(3)	0.17902(2)	0.75614(5)	0.09635(8)	0.00895(17)	1.0
Ta(1)	0.252685(17)	0.49457(3)	0.12154(5)	0.00954(15)	1.0
O(1)	0.2708(3)	0.3437(5)	0.1037(9)	0.0134(14)	1.0
O(2)	0.1720(3)	0.4673(6)	0.0775(9)	0.0100(13)	1.0
O(3)	0.3422(3)	0.5545(6)	0.2025(10)	0.0215(16)	1.0
O(4)	0.2585(4)	0.5205(7)	−0.1195(11)	0.026(2)	1.0
O(5)	0.2479(3)	0.6698(6)	0.1586(9)	0.0134(14)	1.0
O(6)	0.4059(3)	0.3785(6)	0.0673(10)	0.0212(16)	1.0
O(7)	0.4165(4)	0.5907(9)	−0.0561(13)	0.019(3)	0.715(16)
O(8)	0.0737(3)	0.3526(6)	0.0551(10)	0.0177(15)	1.0
O(9)	−0.0443(3)	0.4159(6)	0.0246(11)	0.0230(17)	1.0
O(10)	0.0000	0.2361(11)	0.2500	0.018(4)	0.77(3)
O(11)	0.0000	0.3769(11)	−0.2500	0.017(4)	0.80(3)
O(12)	0.1412(3)	0.6823(6)	0.2582(9)	0.0126(14)	1.0
O(13)	0.1503(3)	0.6818(6)	−0.1194(9)	0.0139(14)	1.0

[a] U_{eq} is defined as one-third of the trace of the orthogonalized U_{ij} tensor.

Ta^{5+} must remain fully occupied. Of the remaining Te^{4+} cations, Te(1*a*)/Te(1*b*) and Te(2) are both four-coordinate whereas Te(3) is three-coordinate. It is also unlikely that Te^{4+} would be two-coordinate; thus all of the oxygen atoms around Te(3) must also be fully occupied. For Te(1*a*) (Te(1*b*)), the bond distances to O(7) and its symmetry equivalent are 1.97(2) Å, (1.91(2) Å) and 2.44(2) Å, (2.51(3) Å), respectively. The latter distance is substantially longer than what is observed normally for Te^{4+}–O bonds, indicating some partial occupancy in O(7). Similarly, for Te(2), the Te(2)–O(10) and Te(2)–O(11) bond distances are longer than typical Te^{4+}–O contacts, suggesting partial occupancy in O(10) and O(11). Thus the most reasonable and structurally sensible model is to refine the occupancies of O(7), O(10), and O(11). In doing so, partial occupancies of 0.715(16), 0.77(3), and 0.80(3) were refined for O(7), O(10), and O(11), respectively.

2.4. Powder diffraction

The X-ray powder diffraction data were collected on a Scintag XDS2000 diffractometer at room temperature (Cu$K\alpha$ radiation, $\theta-\theta$ mode, flat plate geometry) in the 2θ range 3–110° with a step size of 0.02°, and a step time of 10 s. For $La_4Te_6Nb_2O_{23}$, the unit cell was determined by using the program ERACEL [13]. The unit cell, d_{obs}, d_{calc}, I_{obs}, and I_{calc} are given in Table 5.

2.5. Infrared spectroscopy

Infrared spectra were recorded on a Matteson FTIR 5000 spectrometer in the 400–4000 cm^{-1} range, with the sample pressed between two KBr pellets. The infrared spectra of all three materials revealed *M*–O, Te–O, *M*–O–*M*, Te–O–Te, and *M*–O–Te vibrations (*M* = Nb or Ta). The infrared vibrations and assignments are given in Table 6. The assignments are consistent with those previously reported [14–16].

2.6. Thermogravimetric analysis

Thermogravimetric analyses were carried out on a TGA 2950 Thermogravimetric Analyzer (TA Instruments). The samples were contained within platinum crucibles and heated at a rate of 10°C min^{-1} from room temperature to 900°C in nitrogen. No weight losses or phase changes were observed up to 900°C for all three materials.

2.7. Dielectric characterization

The dielectric constant (κ) and quality factor ($Q = 1/\tan\delta$) measurements were performed using a HP4192A impedance analyzer operating at 1 MHz. Polycrystalline $LaTeNbO_6$, $La_4Te_6Nb_2O_{23}$, and

Table 5
Powder X-ray diffraction data for $La_4Te_6Nb_2O_{23}$ [refined unit cell[a] $a = 23.407(4)$ Å, $b = 12.055(2)$ Å, $c = 7.714(1)$ Å, $\alpha = 90°$, $\beta = 101.59(1)°$, $\gamma = 90°$; space group $C2/c$ (No. 15)]

h	*k*	*l*	d_{obs}	d_{calc}	I_{obs}	I_{calc}[a]
2	0	0	11.470	11.465	2	3
−1	1	1	6.458	6.459	4	5
4	0	0	5.734	5.732	1	1
2	2	0	5.336	5.335	1	1
4	2	0	4.156	4.154	4	4
1	3	0	3.959	3.958	4	4
6	0	0	3.821	3.822	1	1
−1	1	2	3.671	3.672	5	5
−1	3	1	3.556	3.557	8	7
1	1	2	3.461	3.461	3	2
−2	2	2	3.229	3.229	45	45
6	2	0	3.227	3.228	100	100
0	2	2	3.202	3.201	27	28
7	1	0	3.162	3.161	4	4
−7	1	1	3.140	3.141	9	9
3	3	1	3.108	3.108	1	1
3	1	2	3.043	3.043	5	4
0	4	0	3.013	3.014	39	39
−6	0	2	3.005	3.006	17	17
2	2	2	2.957	2.956	4	4
2	4	0	2.915	2.915	3	3
4	0	2	2.899	2.898	25	24
6	2	1	2.801	2.801	1	1
−3	3	2	2.720	2.720	4	3
5	3	1	2.687	2.686	1	1
4	4	0	2.668	2.668	1	1
8	2	0	2.589	2.588	3	3
7	3	0	2.539	2.539	3	4
−3	1	3	2.495	2.494	1	1
6	0	2	2.451	2.452	2	2
1	5	0	2.397	2.398	1	2
0	4	2	2.356	2.356	1	1
8	2	1	2.322	2.323	1	1
10	0	0	2.294	2.293	1	1
−4	4	2	2.282	2.282	1	1
2	4	2	2.253	2.253	4	4
5	3	2	2.221	2.221	1	1

Calculated using the atomic coordinates for $La_4Te_6Ta_2O_{23}$ but substituting niobium for tantalum.

[a] The unit cell was determined by using the program ERACEL [13].

Table 6
Infrared vibrations (cm^{-1}) for $LaTeNbO_6$ and $La_4Te_6M_2O_{23}$ (*M* = Nb or Ta)

	M–O	Te–O	*M*–O–*M*	*M*–O–Te	Te–O–Te
$LaTeNbO_6$	917	794 665	750 538	613	472
$La_4Te_6Nb_2O_{23}$	909	781 759 653	723 688 540	610	422
$La_4Te_6Ta_2O_{23}$	912	784 761 653	725 690 532	613	428

$La_4Te_6Ta_2O_{23}$ were pressed into 1.2 cm diameter and 0.15 cm thick pellets and sintered at 900°C for 10 h. The pellets had a density 90% of theoretical. A conducting silver paste was applied to the pellet surfaces for electrodes and cured at 400°C. The temperature dependence of the dielectric constants (TCK) was measured, between −20°C and 100°C, by placing the pellets in a Linkam THMSE600 hot stage.

3. Results and discussion

$LaTeNbO_6$ has a unidimensional crystal structure consisting of parallel chains of corner-shared NbO_6 octahedra. Each NbO_6 octahedron is also linked to a TeO_3 group (see Fig. 1). The Te^{4+} cation is in an asymmetric coordination environment attributable to its stereo-active lone-pair. The parallel chains run along the *b*-axis and are separated by the La^{3+} cations. The Nb–O and Te–O bond distances range from 1.772(7) to 2.391(7) Å and 1.879(6) to 1.924(6) Å, respectively. In connectivity terms, $LaNbTeO_6$ can be formulated as consisting of $\{[TeO_{2/2}O_{1/1}]^0\ [NbO_{4/2}O_{2/1}]^{3-}\}^{3-}$ anionic chains, with charge balance retained by the La^{3+} cations. Bond valence calculations [17,18] resulted in values of 4.75 and 4.93 for Nb^{5+} and 3.61 and 3.86 for Te^{4+}. Interestingly, we were unable to synthesize $LaTeTaO_6$ using the same synthetic method as $LaTeNbO_6$. Although several attempts were made, all efforts to synthesize $LaTeTaO_6$ produced $La_4Te_6Ta_2O_{23}$ and a mixture of reagents. This indicates that if $LaTeTaO_6$ exists at all, the material is extremely unstable with respect to $La_4Te_6Ta_2O_{23}$.

$La_4Te_6M_2O_{23}$ (M = Nb or Ta) also has a unidimensional crystal structure, consisting of different types of chains that run parallel to the *c*-axis (see Fig. 2). One chain consists of corner-linked TaO_6 octahedra. Each TaO_6 octahedron shares additional corners with TeO_3 and TeO_4 groups (see Fig. 3a). Similar to $LaTeNbO_6$, the Te^{4+} cations in $La_4Te_6M_2O_{23}$ (M = Nb or Ta) are also in asymmetric coordination environments attributable to their stereo-active lone-pairs. The TeO_3 polyhedra are separated from each other, but the TeO_4 groups are connected through an oxygen atom (see Fig. 3a). However, this oxygen atom, O(7), is partially occupied (0.715(16)); thus the TeO_4 'chain' is broken at random intervals. In other words, TeO_3 groups are observed. The other chain is similar to the aforementioned TeO_4 unit. This chain also consists of four-coordinate Te^{4+} that share corners through oxygen atoms (see Fig. 3b). However, similar to O(7), these oxygen atoms, O(10) and O(11), are also partially occupied (0.77(3) and 0.80(3), respectively) indicating that this 'chain' is also broken, again resulting in TeO_3 groups. These types of broken chains have been observed previously in $Ga_2Te_4O_{11}$ [19]. Both sets of 'chains' run parallel to the *c*-axis and are separated by La^{3+} cations. In addition, the lone-pair on the Te^{4+} in the two broken chains point toward each other resulting in the formation of small cavities throughout the structure (see Fig. 2). Bond distances for Ta–O and Te–O range from 1.886(8) to 2.151(9) Å and 1.847(9) to 2.221(12) Å, respectively. Bond valence calculations

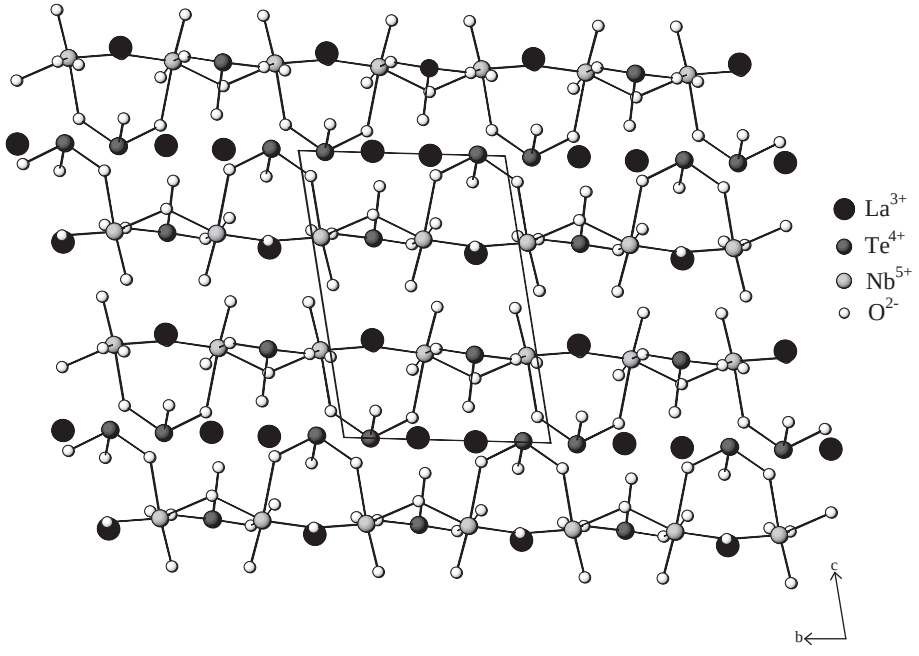

Fig. 1. Ball-and-stick diagram of $LaTeNbO_6$ in the $b-c$ plane.

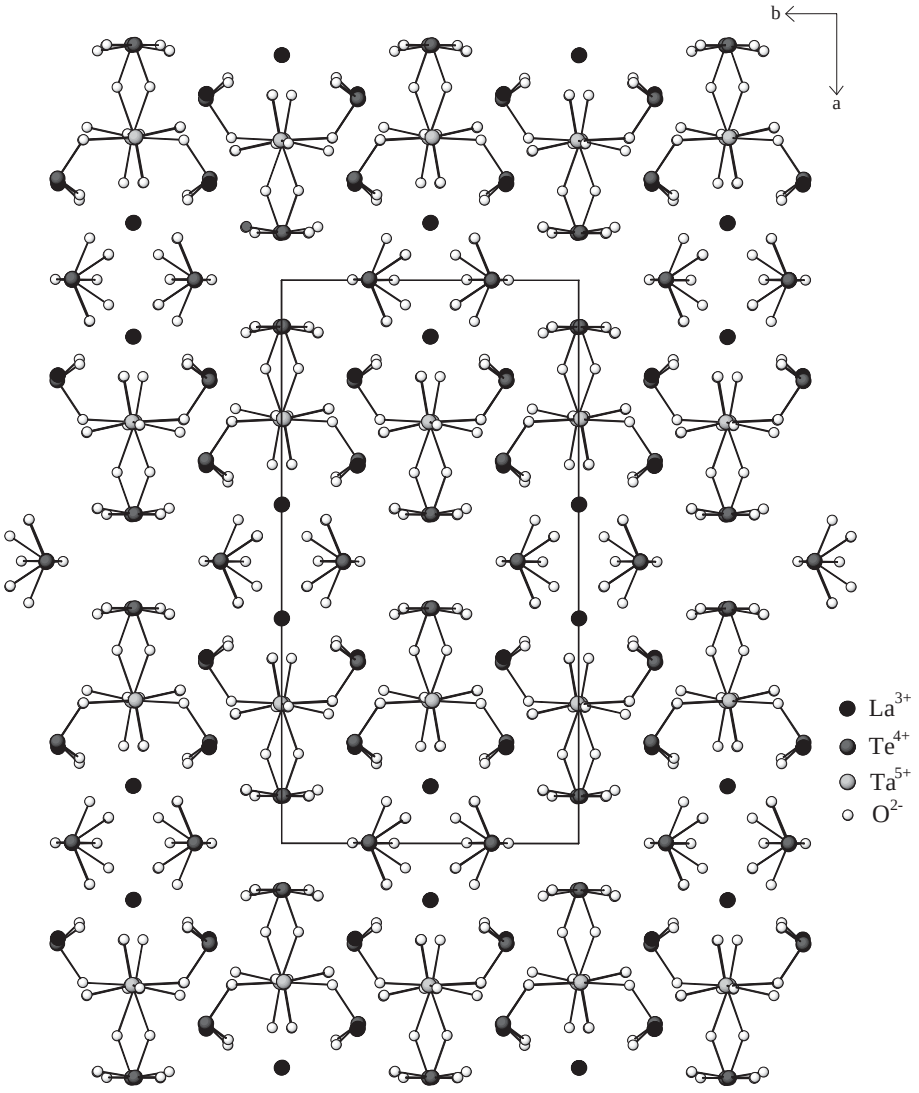

Fig. 2. Ball-and-stick diagram of $La_4Te_6Ta_2O_{23}$ in the $a-b$ plane.

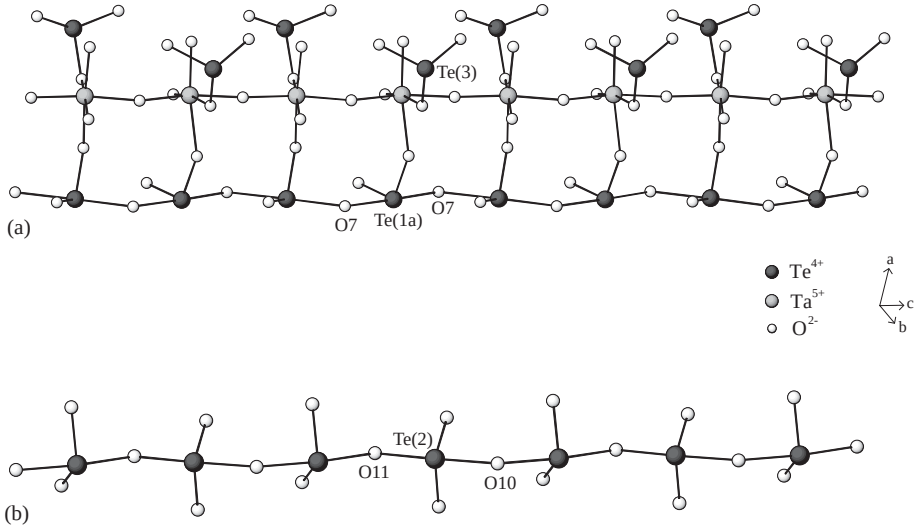

Fig. 3. Ball-and-stick diagram of $La_4Te_6Ta_2O_{23}$ showing the (a) TaO_6 chains and (b) $Te(2)O_4$ 'chains' running along the c-axis. In (a), for clarity, only Te(1a) is shown. Note that O(7), O(10), and O(11) are partially occupied (see text).

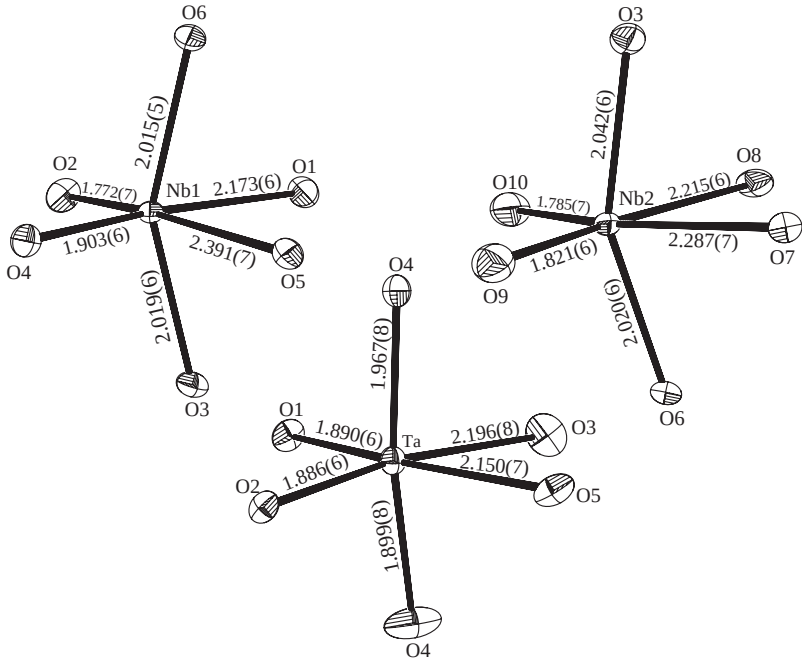

Fig. 4. ORTEP (50% probability ellipsoids) for the Nb^{5+} and Ta^{5+} octahedra in $LaTeNbO_6$ and $La_4Te_6Ta2O_{23}$. Note the intra-octahedral distortion toward the edge (local [110] direction) of each octahedron.

[17,18] resulted in values of 5.14 for Ta^{5+} and 3.78, 3.97, and 4.19 for Te^{4+}.

Although $LaTeNbO_6$ and $La_4Te_6M_2O_{23}$ (M = Nb or Ta) are structurally very different, the local (distorted) coordination environments of the cations are very similar. In all three materials, the M^{5+} (M = Nb or Ta) cation is in a distorted octahedral coordination environment bonded to six oxygen atoms. This cationic displacement can be attributed to a SOJT distortion. Interestingly, all of the intra-octahedral distortions are toward an edge, along the local [110] direction, and results in two 'short', two 'normal', and two 'long' bonds (see Fig. 4). In addition, for all the octahedra the two shortest M^{5+}–O bonds are terminal, whereas the two longest bonds are connected to a Te^{4+} cation. The remaining M^{5+}–O bonds (the 'normal' bonds) bridge to another M^{5+} cation. The Te^{4+} cations are in distorted three- or four-coordinate environments, attributable to their stereo-active lone-pair. Finally, for $LaTeNbO_6$ and $La_4Te_6M_2O_{23}$ (M = Nb or Ta), the La^{3+} cations are in eight- or nine-fold coordination, respectively.

3.1. Dielectric measurements

Since the reported materials contain polarizable cations, i.e. Te^{4+}, Nb^{5+} and Ta^{5+}, we felt it would be interesting to investigate their bulk dielectric properties. The dielectric constant for all three materials are very similar, with $\kappa = 12.9$, 17.0, and 15.9 for $LaTeNbO_6$, $La_4Te_6Nb_2O_{23}$, and $La_4Te_6Ta_2O_{23}$, respectively. With the quality factor ($Q = 1/\tan\delta$) and temperature dependence of the dielectric constant (TCK), it is not surprising that the values for $La_4Te_6Nb_2O_{23}$ and $La_4Te_6Ta_2O_{23}$ are very similar ($Q = 36.8$ and 36.6; TCK = +1730 and +1890 ppm/°C, respectively), attributable to the materials being iso-structural (see Table 7). Interestingly, Q and TCK for $LaTeNbO_6$ are superior to $La_4Te_6M_2O_{23}$ (M = Nb or Ta), possibly owing to the lack of oxygen vacancies in the former material. In addition, variable frequency measurements on $La_4Te_6M_2O_{23}$ (M = Nb or Ta) at 10 kHz, 100 kHz, and 1 MHz between 400°C and 600°C revealed a peak in the dielectric constant, indicating dielectric relaxation phenomena. Additional measurements are underway in order to ascertain the origin of this dielectric behavior.

Table 7
Dielectric constant (κ), quality factor (Q), and temperature coefficient of the dielectric constant (TCK) for $LaTeNbO_6$ and $La_4Te_6M_2O_{23}$ (M = Nb or Ta) at 1 MHz and 20°C

	κ	$Q(1/\tan\delta)$	TCK (ppm/°C)
$LaTeNbO_6$	12.89	>100	+103
$La_4Te_6Nb_2O_{23}$	17.01	36.8	+1730
$La_4Te_6Ta_2O_{23}$	15.91	36.6	+1890

κ, dielectric constant; $Q = 1/\tan\delta$; TCK = $[(\kappa_{100}-\kappa_{-20})/\kappa_{40}]/120$.

Acknowledgments

We thank the Robert A. Welch Foundation for support. We also acknowledge Dr. Xiqu Wang for

crystallographic assistance. This work was also supported by the NSF-Career Program through DMR-0092054 and an acknowledgment is made to the donors of The Petroleum Research Fund, administered by the American Chemical Society, for partial support of this research. P.S.H. is a Beckman Young Investigator.

Supporting information available

Powder X-ray diffraction patterns (calculated and experimental) are available (PDF). Further details of the crystal structure investigation(s) can be obtained from the Fachinformationszentrum Karlsruhe, 76344 Eggenstein-Leopoldshafen, Germany, (fax: (49) 7247-808-666; e-mail: crysdata@fiz.karlsruhe.de) on quoting the depository number CSD-413007 and CSD-413008.

References

[1] U. Opik, M.H.L. Pryce, Proc. Roy. Soc. (London) A 238 (1957) 425.
[2] R.F.W. Bader, Mol. Phys. 3 (1960) 137.
[3] R.F.W. Bader, Can. J. Chem. 40 (1962) 1164.
[4] R.G. Pearson, J. Mol. Struct. (Theochem) 103 (1983) 25.
[5] R.A. Wheeler, M.-H. Whangbo, T. Hughbanks, R. Hoffmann, J.K. Burdett, T.A. Albright, J. Am. Chem. Soc. 108 (1986) 2222.
[6] M. Tatsumisago, T. Minami, Y. Kowada, H. Adachi, Phys. Chem. Glasses 35 (1994) 89.
[7] C.R. Becker, S.L. Tagg, J.C. Huffman, J.W. Zwanziger, Inorg. Chem. 36 (1997) 5559.
[8] J. Goodey, K.M. Ok, J. Broussard, C. Hofmann, F.V. Escobedo, P.S. Halasyamani, J. Solid State Chem., 2003, in press.
[9] SAINT, Version 4.05, Siemens Analytical X-ray Instruments, Inc., Madison, WI, 1995.
[10] G.M. Sheldrick, SHELXS-97, Program for the Automatic Solution of Crystal Structures, University of Goettingen, Goettingen, Germany, 1997.
[11] G.M. Sheldrick, SHELXL-97, Program for the Refinement of Crystal Structures, University of Goettingen, Goettingen, Germany, 1997.
[12] L.J. Farrugia, J. Appl. Crystallogr. 32 (1999) 837.
[13] J. Laugier, A. Filhol, ERACEL, Program for the Refinement of Cell Parameters, 1978.
[14] D.A. Judd, Q. Chen, C.F. Campana, J. Am. Chem. Soc. 119 (1997) 5461.
[15] G.-S. Kim, H. Zeng, D. VanDerveer, C.L. Hill, Angew. Chem. Int. Ed. 38 (1999) 3205.
[16] K.M. Ok, P.S. Halasyamani, Chem. Mater. 13 (2001) 4278.
[17] I.D. Brown, D. Altermatt, Acta Crystallogr. B 41 (1985) 244.
[18] N.E. Brese, M. O'Keeffe, Acta Crystallogr. B 47 (1991) 192.
[19] M. Dutreilh, P. Thomas, J.C. Champarnaud-Mesjard, B. Frit, Solid State Sci. 3 (2001) 423.